9. Yoshizu A, Izumi Y, Park S, Sakai H, Takeoka S, Horinouchi H, Ikeda E, Tsuchida E, Kobayashi K. Hemorrhagic shock resuscitation with an artificial oxygen carrier, hemoglobin vesicle, maintains intestinal perfusion and suppresses the increase in plasma tumor necrosis factor-alpha. ASAIO J 2004;50:458–463
10. Sakai H, Masada Y, Horinouchi H, Yamamoto M, Ikeda E, Takeoka S, Kobayashi K, Tsuchida E. Hemoglobin vesicles suspended in recombinant human serum albumin for resuscitation from hemorrhagic shock in anesthetized rats. Crit Care Med 2004;32:539–545
11. Takahashi A. Characterization of neo red cells (NRCs), their function and safety in in vivo tests. Artif Cells Blood Substit Immobil Biotechnol 1995;23:347–354
12. Ogata Y, Goto H, Kimura T, Fukui H. Development of neo red cells (NRC) with the enzymatic reduction system of methemoglobin. Artif Cells Blood Substit Immobil Biotechnol 1997;25: 417–427
13. Wasserman K, Beaver WL, Davis JA, Pu JZ, Heber D, Whipp BJ. Lactate, pyruvate, and lactate-to-pyruvate ratio during exercise and recovery. J Appl Physiol 1985;59:935–940
14. Wasserman K, Beaver WL, Whipp BJ. Gas exchange theory and the lactic acidosis (anaerobic) threshold. Circulation 1990;81: II14–30

Effect of Systolic Duration on Mechanical Heart Valve Cavitation in a Pneumatic Ventricular Assist Device: Using a Monoleaflet Valve

HWANSUNG LEE, EISUKE TATSUMI, AND YOSHIYUKI TAENAKA

The cavitation intensity of a mechanical heart valve (MHV) may differ according to the geometry of the blood pump and driving mechanism. Our group is currently developing a pneumatic ventricular assist device (VAD), and the effects of different operating conditions on MHV cavitation in our pneumatic VAD were investigated. Tests were conducted under physiological pressure at heart rates ranging from 60 to 90 beats/min and at a systolic duration ranging from 38% to 43%. The valve-closing velocity was measured using a charge-coupled device (CCD) laser displacement sensor, and images of MHV cavitation were recorded using a high-speed video camera. A miniature pressure sensor was mounted 10 mm away from the inlet valve surface. The data were stored at a 1-MHz sampling rate using a digital oscilloscope. The pressure signal was band-pass filtered between 35 and 200 kHz using a digital filter. The cavitation bubbles were concentrated at the inlet valve stop, and were caused mainly by the squeeze flow. The band-pass filtered root mean squared (RMS) pressure and cavitation cycle duration increased with the closing velocity of the inlet valve. At a low heart rate and low systolic duration, the inlet valve closed before the outlet valve opened, which caused no cavitation bubbles to form around the valve stop. *ASAIO Journal* 2008; 54:25–30.

Cavitation is the rapid formation of vaporous bubbles caused by a transient reduction in pressure below liquid vapor pressure, and the rapid collapse of these bubbles during pressure recovery.[1] Cavitation bubble collapse also leads to high shear stresses, which may have a more significant effect on hemolysis than does high pressure. In general, the causes of cavitation in mechanical heart valves (MHVs) include the venture effect caused by flow after valve closure in the narrow gap between the leaflet and valve housing, the water hammer effect caused by the sudden stop of the valve, and the squeeze flow that can occur in the narrow gap between the leaflet and valve stop during the final period of valve closure. Recently, squeeze flow was noted to be a major cause of cavitation in the MHV.[2–7] In previous studies, we investigated MHV cavitation intensity and its mechanism in an electro-hydraulic total artificial heart.[8–10] We reported that most of the cavitation bubbles were observed around the valve stop and were caused by the squeeze flow, and that the formation of cavitation bubbles depended on the valve-closing velocity and valve leaflet geometry.[8] The valve-closing velocity and valve stop area of the bileaflet valve were less than that of the Medtronic-Hall monoleaflet valve, resulting in less cavitation intensity of the bileaflet valves.[9,10] The observation time of the cavitation bubbles (herein, the cavitation cycle duration) was closely related to the valve-closing velocity, and hence the cavitation cycle duration was used for determining the MHV cavitation intensity.[8–10] However, this method does not account for size of the cavitation bubbles.

In our laboratory, we have been developing a diaphragm-type pneumatic ventricular assist device (VAD). The Medtronic Hall monoleaflet valve has excellent durability, very good hemodynamic performance, and exceptionally low thrombogenicity, leading to good long-term survival with low complication rates.[11] In addition, we assumed that the flow through the major orifice of the monoleaflet valve acted on the blood pump in some way, which is good for the washout effect inside the blood pump, resulting in the prevention of thrombosis. For those reasons, the Medtronic Hall monoleaflet valve using a monoleaflet valve was used in our pneumatic VAD. The Medtronic Hall monoleaflet valves were rigidly mounted in the valve port made of polyurethane. Because the valve port has no compliance beyond that used in a clinical context, the greater cavitation intensity might occur. The purpose of this study was to investigate the MHV cavitation intensity under different running conditions of our pneumatic VAD. First of all, to estimate the effect of systolic duration on MHV cavitation intensity in our pneumatic VAD, the hemodynamic characteristics of the MHV were investigated.

Materials and Methods

A diaphragm-type pneumatic VAD was developed by the National Cardiovascular Center in Japan[12] (**Figure 1**). This VAD has an outer diameter of 88 mm, a thickness of 47 mm, and a stroke volume of 75 ml. The pneumatic VAD was connected to a Donovan mock circulatory loop tester. A 23-mm Medtronic Hall monoleaflet valve (Medtronic, Inc., Minneapolis, MN) was mounted in the mitral and aortic positions on a 90 degrees inclined plane in our pneumatic VAD after removing the sewing ring. Our pneumatic VAD was operated at a positive pressure ranging from 180 to 220 mm Hg and a negative pressure ranging from −30 to −60 mm Hg,

From the Department of Artificial Organs, Research Institute, National Cardiovascular Center, Osaka, Japan.

Submitted for consideration May 2007; accepted for publication in revised form July 2007.

Reprint Requests: Hwansung Lee, PhD, Department of Artificial Organs, The Advanced Medical Engineering Center, Research Institute, National Cardiovascular Center, 5-7-1, Fujishiro-dai, Suita, Osaka 565-8565, Japan.

DOI: 10.1097/MAT.0b013e318161d71c

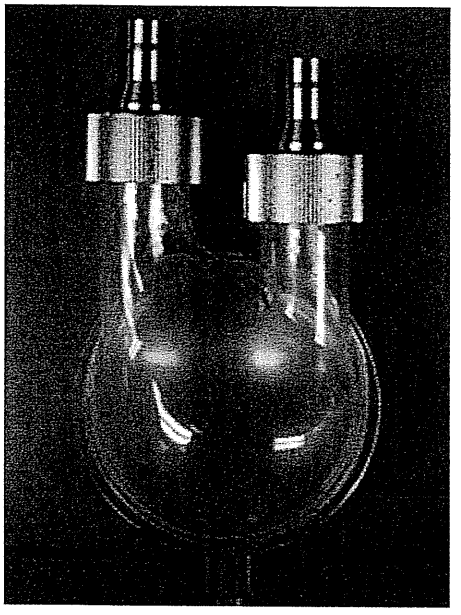

Figure 1. Photograph of the pneumatic ventricular assist device which has been under development in our laboratory. It has an outer diameter of 88 mm, a thickness of 47 mm, and a stroke volume of 75 ml.

using a control-drive console for circulatory support (VCT-30; Toyobo, Osaka, Japan), which ran at heart rates ranging from 60 to 90 beats/min, and at systolic duration ranging from 38% to 43%. Mean aortic and atrial pressures were maintained at 100 mm Hg and 7 mm Hg, respectively. The blood analog fluid was a mixture of 50% water and 50% glycerol by volume, which has a viscosity coefficient of 3.4 cP, a density of 1.12 g/cm^3, and a vapor pressure of −715 mm Hg at 37°C.

A charge-coupled device (CCD) laser displacement sensor (LC-2450; Keyence, Osaka, Japan) with a frequency sampling rate of 50 kHz was used to detect the closing motion of the valve leaflet (**Figure 2**). The chamber was constructed of acrylic resin for optical access and a laser displacement sensor was placed on top of the acrylic chamber (**Figure 2**). A high-speed camera (fx-6000; NAC, Tokyo, Japan) was also placed on top of the acrylic chamber, and images of the cavitation bubbles were recorded at 30,000 frames per second.

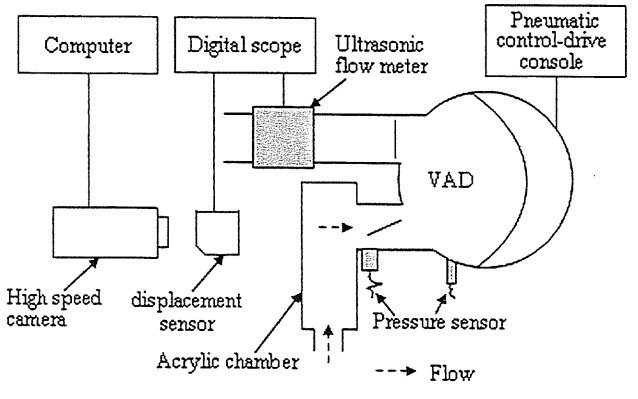

Figure 2. Diagram of the experimental system.

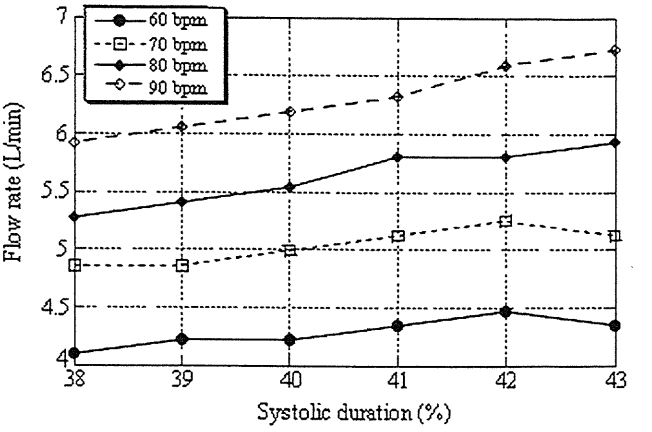

Figure 3. Flow rate at various heart rates and systolic durations.

A miniature pressure sensor (105C02, PCB Piezotronics, Depew, NY) with a resonance frequency of 250 kHz was mounted 10 mm away from the valve surface. The data were stored using a digital oscilloscope (DL1640L, Yokogawa, Tokyo, Japan) at a 1-MHz sampling rate. The pressure signal was band-pass filtered between 35 and 200 kHz using a digital filter, and the power spectrum of the pressure signal used a digital Fast Fourier Transform (FFT) (Labview 7.0, National Instruments, Austin, TX).

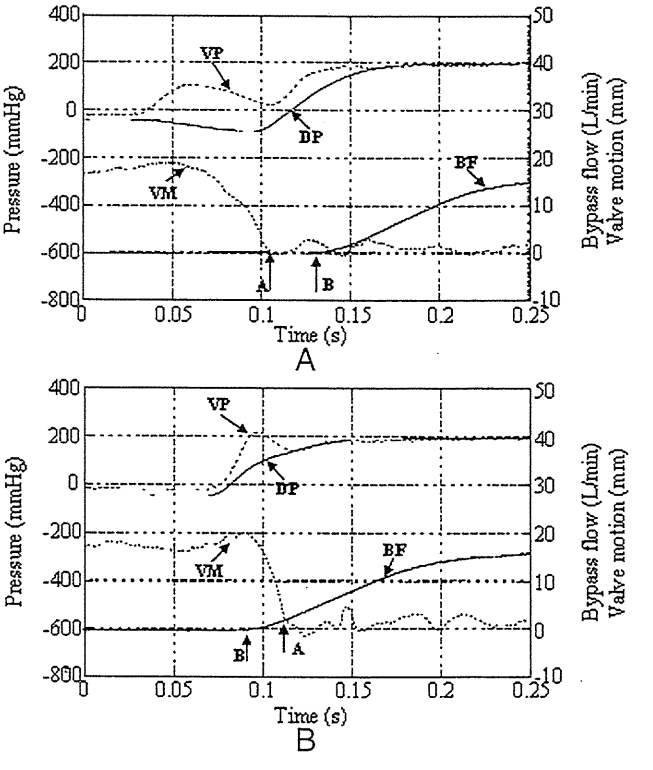

Figure 4. Waves of flow rate, valve motion, and ventricular and driving pressures at a heart rate of 80 bpm. (A) systolic duration of 38%, (B) systolic duration of 42%. VP, ventricular pressure; DP, driving pressure; VM, valve motion; BF, bypass flow; A, inlet valve closed; B, outlet valve open.

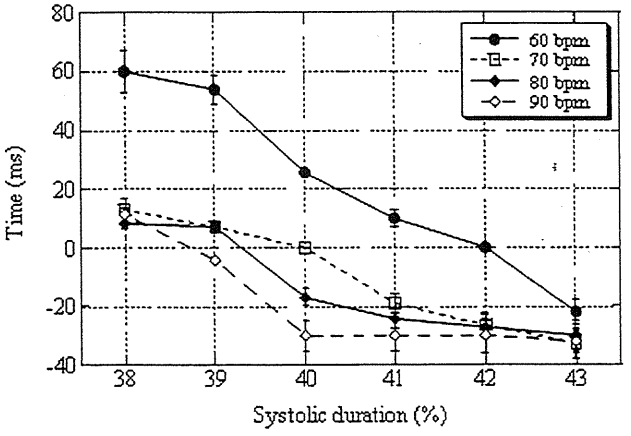

Figure 5. Timing interval between the inlet valve closing and outlet valve opening. A positive value of this interval indicates that the inlet valve closed before the outlet valve opened.

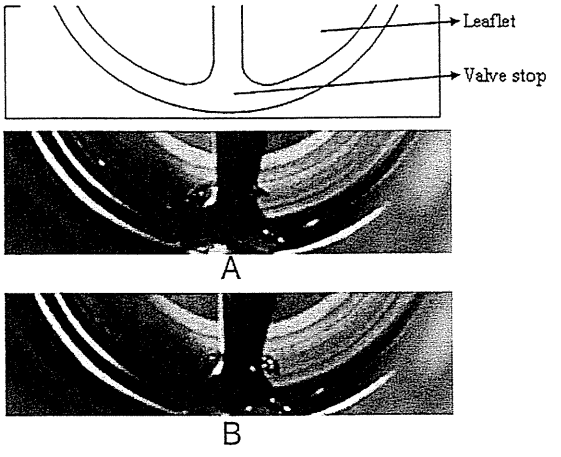

Figure 7. Cavitation bubbles at a heart rate of 70 beats/min. (A) systolic duration of 41%, (B) systolic duration of 43%.

Results

The bypass flow of the pneumatic VAD ranged from 4.1 to 6.7 L/min (**Figure 3**). In low systolic duration, the blood pump performs partial-filling and partial-ejection. On the other hand, in high systolic duration the blood pump performs full-filling and full-ejection.

The flow rate, valve motion, and driving pressure signal at a heart rate of 80 bpm are shown in **Figure 4**. The start of the outlet flow was defined as the moment at which the outlet valve opened. Point "A" in **Figure 4** indicates the point at which the inlet valve closed, and "B" indicates the point at which the outlet valve opened. The outlet valve opened after the inlet valve closed when the systolic duration reached 38% (**Figure 4A**). When the outlet valve opened after the inlet valve closed, the ventricular pressure showed a small peak value (**Figure 4A**). On the other hand, when the outlet valve opened before the inlet valve closed, the ventricular pressure had a large peak value (**Figure 4B**). When the outlet valve opened after the inlet valve closed, the timing interval was defined as a positive value; its value ranged from 60 ± 5.7 to −40 ± 2.5 milliseconds (**Figure 5**). During a high heart rate and high systolic duration, the outlet valve opened before the inlet valve closed.

The valve-closing velocity during 5 milliseconds just before valve closure is shown in **Figure 6**. The valve-closing velocity increased as the heart rate and systolic duration increased, and the velocity ranged from 0.64 ± 0.15 to 1.25 ± 0.23 m/s (**Figure 6**).

Most cavitation bubbles were concentrated near the valve stop (**Figures 7** and **8**). The number of cavitation bubbles increased as the heart rate and the systolic duration increased. The cavitation cycle duration was recorded and the number of frames in which cavitation bubbles were visible counted (**Figure 9**). When the timing interval was a positive value (**Figure 5**), cavitation bubbles were not observed near the valve stop.

The unfiltered and filtered pressure signals are shown in **Figures 10** and **11**. A higher frequency was caused by contact with the valve stop (**Figures 10B** and **11B**). In the case of low heart rate and low systolic duration, the higher frequency caused by cavitation bubbles was not observed (**Figure 10**). However, in the case of high heart rate and high systolic duration, a high frequency ranging between 50 and 100 kHz

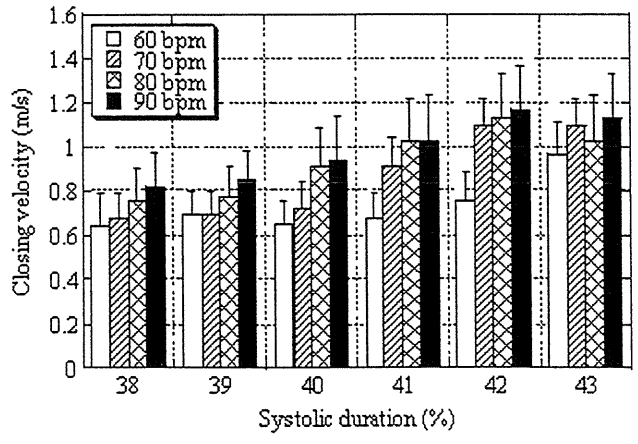

Figure 6. Valve-closing velocity. This closing velocity is the average velocity during the 5 ms just before valve closure.

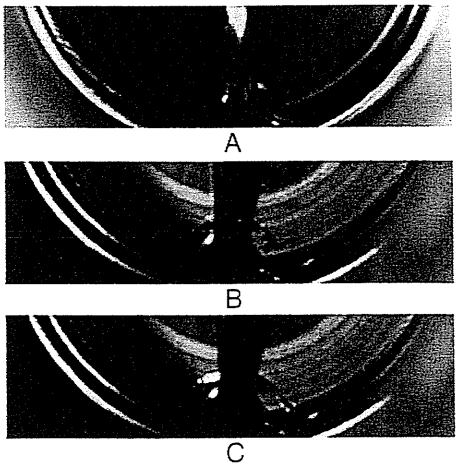

Figure 8. Cavitation bubbles at a heart rate of 90 beats/min. (A) systolic duration of 39%, (B) systolic duration of 41%, (C) systolic duration of 43%.

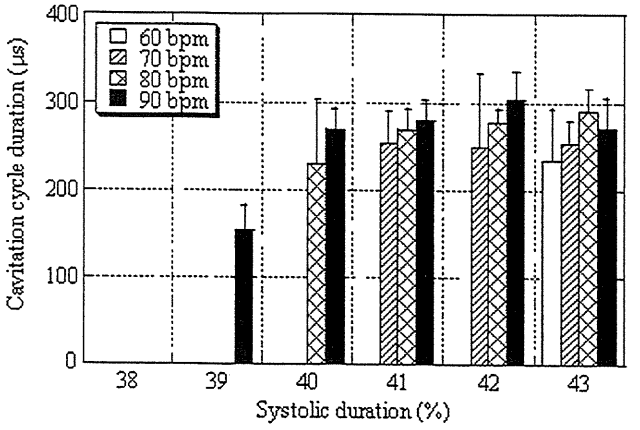

Figure 9. The cavitation cycle duration. The cavitation cycle duration is equal to the number of frames during which cavitation bubbles were visible multiplied by the interval of the frames.

was observed, which might be caused by the collapse of the cavitation bubbles (**Figure 11**).

The relationship between the root mean squared (RMS) pressure of the filtered pressure signal and the valve closing velocity is shown in **Figure 12**. The RMS pressure increased linearly as the valve-closing velocity increased (**Figure 12**). Even if the cavitation bubbles caused by the valve stop were not observed, there occurred an RMS pressure below 10 mm Hg. The cavitation cycle duration increased suddenly above 0.8 m/s of the valve-closing velocity.

Discussion

Lukic *et al.*[13] reported that cavitation intensity was minimal when the pump had immediately completed filling a pediatric pulsatile pneumatic VAD with stroke volume ranges from 10 to 15 ml. In a previous study, we reported that the cavitation intensity of partial-filling and partial-ejection was less than that of the full-filling and full-ejection condition in an electro-hydraulic total artificial heart.[10,14] Moreover, in the present study, the cavitation cycle duration was shorter when systolic duration was short. Even if differences exist between the blood pump geometry and the driving mechanism of the blood pump, the blood pump shows low cavitation intensity in the partial-filling and the partial-ejection condition. Comparing the heart rate of 80 bpm and systolic duration of 38% with the heart rate of 70 bpm and systolic duration of 42%, even if those have the same bypass flow (**Figure 3**), the lower systolic duration of 38% has low closing velocity (**Figure 6**) and no cavitation (**Figure 9**). It means that, even if the heart rate increases, low systolic duration contributes to low closing velocity of the leaflet and then causes no cavitation. Moreover, we could be comparing the heart rate of 90 bpm and systolic duration of 39% with heart rate of 90 bpm and systolic duration of 42%. Even if the bypass flow decreased 8.2% at the low systolic duration (**Figure 3**), the cavitation cycle duration de-

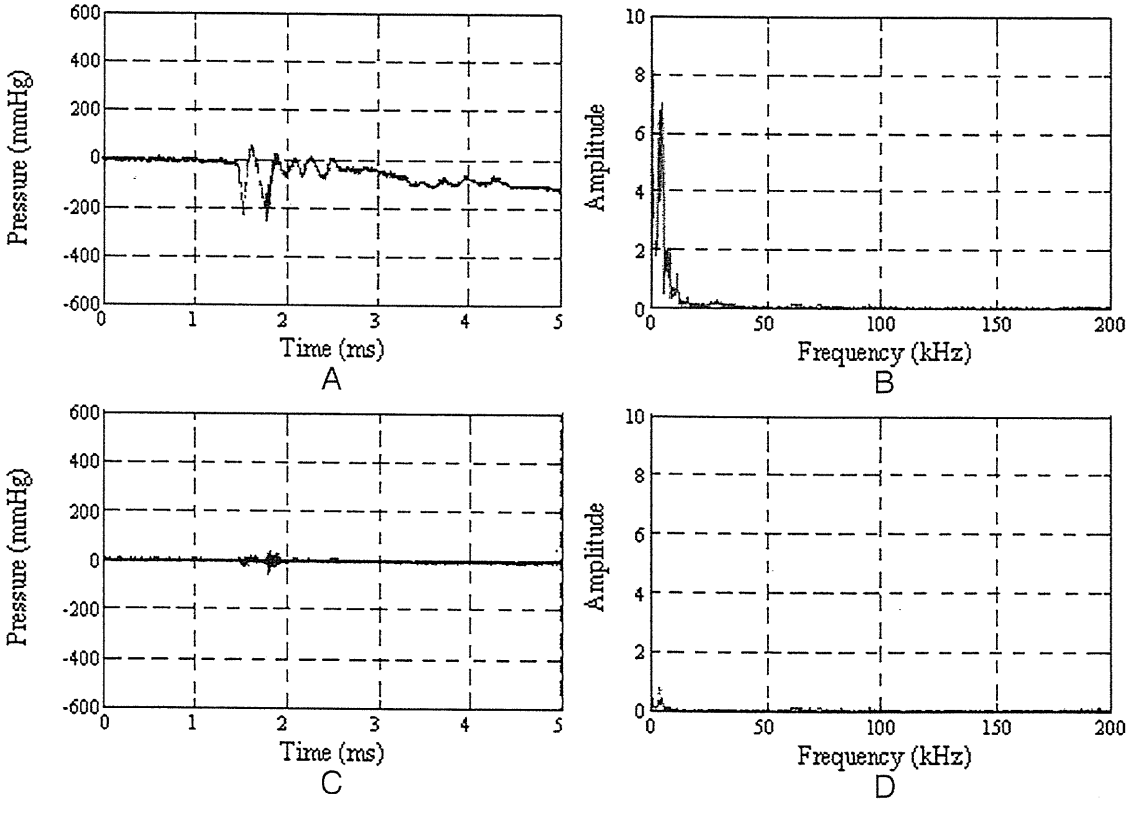

Figure 10. Pressure signal near the inlet valve surface at heart rate of 60 bpm and systolic duration of 38%. (A) unfiltered pressure signal, (B) unfiltered power spectrum, (C) filtered pressure signal, (D) filtered power spectrum. The pressure signal contained valve resonance frequency below 30 kHz. The pressure signal was band-pass filtered between 35 and 200 kHz using a digital filter, which high frequency associated with cavitation bubbles fluctuations.

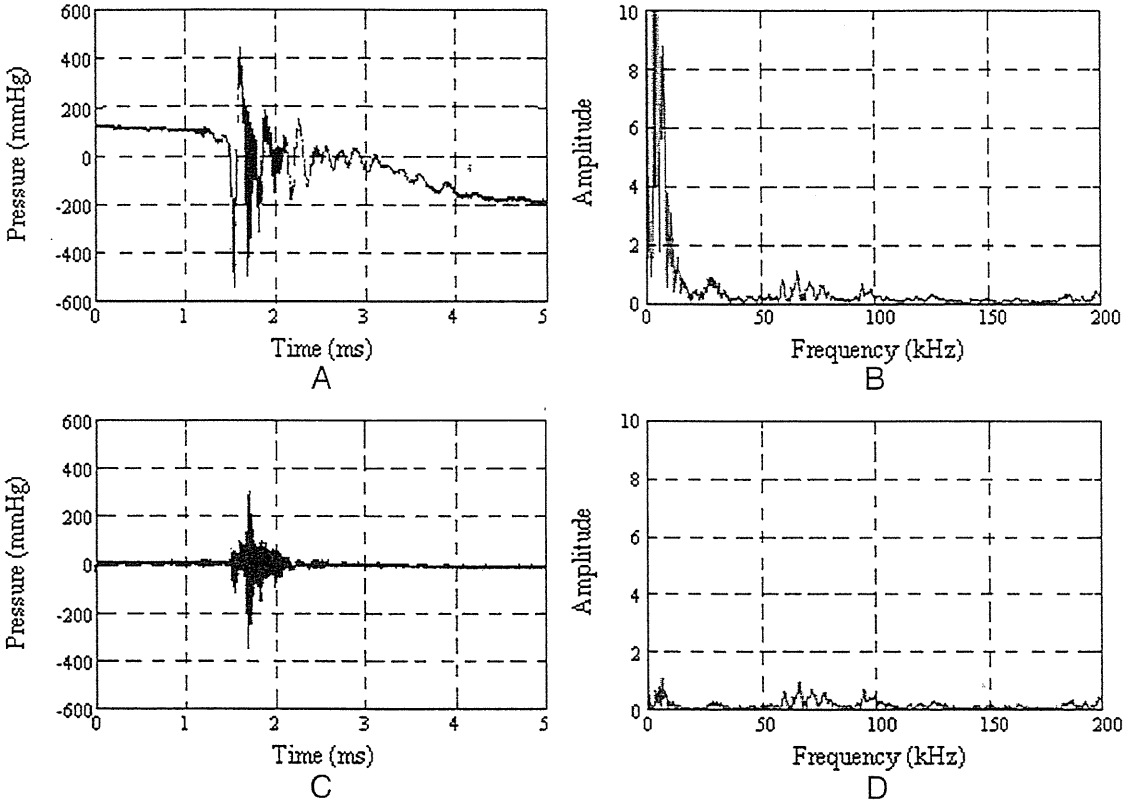

Figure 11. Pressure signal near the inlet valve surface at a heart rate of 90 bpm and a systolic duration of 42%. A: Unfiltered pressure signal, (B) unfiltered power spectrum, (C) filtered pressure signal, (D) filtered power spectrum.

creased 50% (**Figure 9**). In regard to cavitation, even if the bypass flow was decreased, the low systolic duration contributed to the prevention of blood cell trauma.

The full-filling and full-ejection was best condition for the blood pump efficiency and washout effect inside of the blood pump; however, diaphragm is in tension and then will be detrimental to pump durability. However, in the partial-filling and partial-ejection condition, there existed the possibility of thrombosis in the blood pumps inside and around the MHV. Now, we have been constructing the model VAD made of acrylic resin, which has the same geometry as the pneumatic VAD. We will investigate the velocity field of the blood pumps using the visualization method and cavitation intensity for a different running condition of the pneumatic VAD.

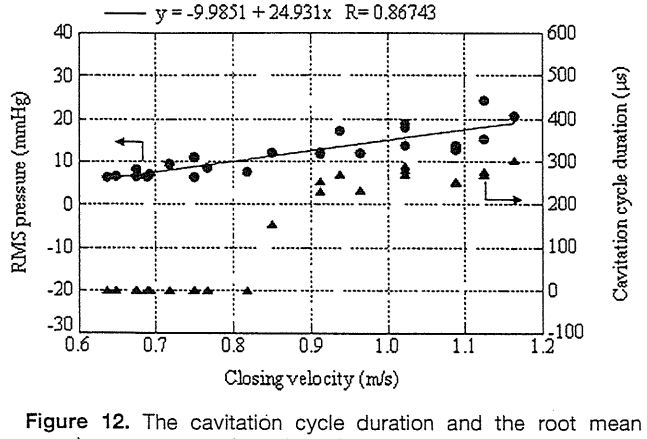

Figure 12. The cavitation cycle duration and the root mean squared pressure at various the valve-closing velocityies.

The US Food and Drug Administration recommended calculating d*P*/d*t* by a linear regression of the transvalvular pressure difference during the last 20 milliseconds before closure when performing cavitation experiments.[15] In the present study, the ventricular pressure pattern at the end-diastolic phase differs from the inlet and outlet valve motion. In all experimental conditions, the ventricular pressure expressed a small peak value before the inlet valve closure (**Figure 4**). Because the ventricular pressure decreased just before the inlet valve closure, we could not estimate the valve-closing velocity using the slope of the ventricular pressure (d*P*/d*t*) during the last 20 milliseconds before valve closure. This means that the slope of the ventricular pressure (d*P*/d*t*) cannot be applied to estimate the cavitation intensity in our pneumatic VAD. However, in this study, we found that cavitation bubbles occur regardless of the ventricular pressure pattern. As shown in **Figure 4**, during full-filling and full-ejection, the peak pressure of the ventricular excess occurred during maximum driving pressure. Therefore, the ventricular pressure pattern might be used to estimate the driving condition of the blood pump and the conditions in which cavitation occurs.

Generally, MHV cavitation has been investigated by means of frequency analysis,[7,16] and RMS pressure has been used as an index of MHV cavitation intensity.[13,17–19] Even if small RMS pressure was detected (**Figure 12**), FFT analysis did not reveal high frequencies (**Figure 10**). The small RMS pressure might occur because of pressure noise. This means that RMS pressure

could not be used as an index for the occurrence of cavitation. However, as the RMS pressure increased with the closing velocity (**Figure 12**), an increase in pressure occurred because of the collapse of the cavitation bubbles. The valve-closing velocity of the Medronic Hall monoleaflet valve in our pneumatic VAD produces a cavitation threshold and an RMS pressure of approximately 0.85 m/s and 10 mm Hg, respectively (**Figure 12**). Most of the cavitation bubbles were concentrated near the valve stop, which is a major cause of squeeze flow. The squeeze flow and cavitation intensity depended on the valve-closing velocity.[10] Moreover, the cavitation threshold of the valve-closing velocity and the RMS pressure differs according to the type of MHV and blood pump geometry. Therefore, as an index of the cavitation threshold, the RMS pressure as well as the valve-closing velocity must be investigated in the development of a pulsatile artificial heart.

Conclusion

In this study, the effect of systolic duration on MHV cavitation intensity in the VAD was investigated. The inlet and outlet valve motion depended on the running condition of our pneumatic VAD. When at a low systolic condition, the inlet valve closed before the outlet valve opened, and cavitation bubbles were not observed on the valve surface. In our pneumatic VAD, systolic duration was found to play an important role in our estimation of whether or not cavitation would occur. These results provide convincing evidence that low systolic duration is safer for the prevention of blood cell damage and valve surface erosion.

Acknowledgments

This work was supported by the Program for Promotion of Fundamental Studies in Health Science of the National Institute of Biomedical Innovation (NIBIO) and Grant-in-Aid for Scientific Research in Japan Society for the Promotion of Science (JSPS) (No.19650120).

References

1. Knapp RT, Daily JW, Hammitt FG: *Cavitation*. Iowa City, Institute of Hydraulic Research, University of Iowa, 1979.
2. Wu ZJ, Wang Y, Hwang NHC: Occluder closing behavior: A key factor in mechanical heart valve cavitation. *J Heart Valve Dis* 3: 25–34, 1994.
3. Makhijani VB, Yang HQ, Singhal AK, Hwang NHC: An experimental computational analysis of MHV cavitation: Effects of leaflet squeezing and rebound. *J Heart Valve Dis* 3: 35–48, 1994.
4. Potthast K, Erdönmen G, Schnelke C, *et al*: Origin and appearance of HITS induced by prosthetic heart valves: An in vitro study. *Int J Artif Organs* 23: 441–445, 2000.
5. Biancucci BA, Deutsch S, Geselowitz DB, Tarbell JM: In vitro studies of gas bubble formation by mechanical heart valves. *J Heart Valve Dis* 8: 186–196, 1999.
6. Zapanta CM, Stinebring DR, Sneckenberger DS, *et al*: In vivo observation of cavitation on prosthetic heart valves. *ASAIO J* 42: 550–555, 1996.
7. Sneckenberger DS, Stinebring DR, Deutsch S, *et al*: Mitral heart valve cavitation in an artificial heart environment. *J Heart Valve Dis* 5: 216–227, 1996.
8. Lee HS, Tsukiya T, Homma A, *et al*: Observation of cavitation bubbles in monoleaflet mechanical heart valves. *J Artif Organs* 7: 121–127, 2004.
9. Lee HS, Taenaka Y, Kitamura S: Mechanisms of mechanical heart valve cavitation in an electrohydraulic total artificial heart. *ASAIO J* 51: 208–213, 2005.
10. Lee HS, Eisuke Tatsumi, Akihiko Homma, *et al*: Mechanism for cavitation of monoleaflet and bileaflet valves in an artificial heart. *J Artif Organs* 9: 154–160, 2006.
11. Butchart EG, Li HH, Payne N, *et al*: Twenty years' experience with the Medtronic Hall valve. *J Thorac Cardiovasc Surg* 121: 1090–1100, 2001.
12. Akagawa E, Lee HS, Tatsumi E, *et al*: Effects of mechanical valve orifice direction on flow pattern in a ventricular assist device. *J Artif Organs* 10: 85–91, 2007.
13. Lukic B, Zapanta CM, Griffith KA, Weiss WJ: Effect of the diastolic and systolic duration on valve cavitation in a pediatric pulsatile ventricular assist device. *ASAIO J* 51: 546–550, 2005.
14. Lee HS, Taenaka Y, Kitamura S: Estimation of mechanical heart valve cavitation in an electro-hydraulic total artificial heart. *Artif Organs* 30: 16–23, 2006.
15. Herman BA, Carey RF: A protocol for the evaluation of the cavitation potential of mechanical heart valves. *J Heart Valve Dis* 3: 128–132, 1994.
16. Wu ZJ, Slonin JH, Hwang NHC: Transient pressure signal in mechanical heart valve cavitation. *ASAIO J* 42: 555–561, 1996.
17. Zapanta CM, Stinebring DR, Deutsch S, *et al*: A comparison of the cavitation potential of prosthetic heart valves based on valve closing dynamics. *J Heart Valve Dis* 7: 655–667, 1998.
18. Wu ZJ, Gao BZ, Hwang NHC: Transient pressure at closing of a monoleaflet mechanical heart valve prosthesis: Mounting compliance effect. *J Heart Valve Dis* 4: 553–567, 1995.
19. Sohn K, Manning KB, Fontaine AA, *et al*: Acoustic and visual characteristics of cavitation induced by mechanical heart valves. *J Heart Valve Dis* 14: 551–558, 2005.

J Artif Organs (2008) 11:60–66
DOI 10.1007/s10047-008-0408-5

ORIGINAL ARTICLE

Hwansung Lee, PhD · Eiki Akagawa, PhD
Eisuke Tatsumi, MD, PhD
Yoshiyuki Taenaka, MD, PhD

Characteristics of cavitation intensity in a mechanical heart valve using a pulsatile device: synchronized analysis between visual images and pressure signals

Abstract To investigate the characteristics of cavitation intensity, we performed a synchronized analysis of the visual images of cavitation and the pressure signals using a pulsatile device. The pulsatile device employed was a pneumatic ventricular assist device (PVAD) that is currently being developed by our group. A 23-mm Medtronic Hall valve (M-H valve) and a 23-mm Sorin Bicarbon bileaflet valve (S-B valve) were mounted in the inlet port of the PVAD after the sewing ring had been removed. A function generator provided a square signal, which was used as the trigger signal, via Electrocardiogram R wave (ECG-R) mode, of the control – drive console for circulatory support. The square signal was also used, after a suitable delay, to synchronize operation of a pressure sensor and a high-speed video camera. The data were stored using a digital oscilloscope at a 1-MHz sampling rate, and then the pressure signal was band-pass filtered between 35 and 200 kHz using a digital filter. The valve-closing velocity, visual cavitation time, and root mean square (RMS) pressure of the M-H valve were greater than those of the S-B valve. Both the visual cavitation time and RMS pressure represent the cavitation intensity, and this is a very important factor when estimating mechanical heart valve cavitation intensity in an artificial heart.

Key words Pneumatic ventricular assist device · Mechanical heart valve · Cavitation

Introduction

Currently over 170000 mechanical heart valves (MHVs) are implanted worldwide each year.[1] MHVs are made of pyrolytic carbon, a hard material, resulting in cavitation generated during valve closure and rebound. Cavitation is the rapid formation and collapse of vapor-filled cavities that occur when a fluid is exposed to rapid changes in pressure below the liquid vapor pressure.[2,3] The collapse of cavitation bubbles causes a high-speed microjet and shock waves, resulting in the generation of high pressure. This high pressure causes blood cell damage,[4] erosion of the leaflet surface, and valve failure.[5] Klepetko et al. observed microscopic pitting on a bileaflet valve at 36 and 38 months after implantation.[5]

In our previous studies, we investigated MHV cavitation in an electrohydraulic total artificial heart (EHTAH).[6] We reported that most of the cavitation bubbles were observed around the valve stop and were caused by the squeeze flow, and that the formation of cavitation bubbles depended on the valve-closing velocity just before valve closure and the valve leaflet geometry.[6] As it relates to squeeze flow, the observed duration of the cavitation bubbles (herein, the visual cavitation time) is closely related to the valve-closing velocity, and hence the visual cavitation time is a valid parameter for determining the MHV cavitation intensity. However, this method does not account for the size of cavitation bubbles. Other research groups have suggested that high-intensity transient pressure detected by ultrasonography is useful as an indication of cavitation intensity.[7–12] However, the frequency of the pressure signal varies widely. Therefore, it is difficult to distinguish the pressure that occurs due to cavitation bubble collapse and that occurring due to the noise of the valve making contact with the valve stop. Another group investigated the characteristics of cavitation intensity, synchronizing analysis between the cavitation visual image and the pressure signal of cavitation bubble collapse using a nonpulsatile device.[13] Because their results were obtained using a nonpulsatile device, it would be difficult to apply their estimates of the characteristics of the cavitation intensity in an in vivo study.

The flow through the major orifice of the Medtronic Hall valve (M-H valve, a monoleaflet valve), when installed in an artificial heart, acted on the blood pump at the diaphragm

Received: November 15, 2007 / Accepted: February 23, 2008

H. Lee (✉) · E. Akagawa · E. Tatsumi · Y. Taenaka
Department of Artificial Organs, Research Institute, National Cardiovascular Center 5-7-1 Fujishiro-dai, Suita 565-8565, Japan
Tel. +81-6-6833-5004 ext. 2368; Fax +81-6-6835-5406
e-mail: hslee@ri.ncvc.go.jp

– housing junction, which was good for the washout effect inside the blood pump, resulting in the prevention of thrombosis. For these reasons, we previously used the M-H valve in an artificial heart. However, the M-H valve is no longer commonly used in clinical settings, and it is possible that it will become unavailable in the near future. MHVs are mounted on a rigid structure by use of a blood pump port made of polyurethane. The valve housings of bileaflet MHVs are made of pyrolytic carbon. Although pyrolytic carbon is a hard material, it is weak against compression stress.[14] Therefore, if compressive stresses act on a valve housing made of pyrolytic carbon, the opening and closing motion of the leaflet might be disturbed. The housing of the Sorin Bicarbon bileaflet valve (S-B valve) is made of a carbofilm-coated titanium alloy, and titanium is able to withstand considerable compressive stress. Moreover, in a previous study, we reported that the S-B valve has a low closing velocity and low cavitation intensity.[15]

In another previous study, we found the valve orientation angle that produced the optimum washout effect inside the blood pump.[16] In this study, the valve orientation angle was fixed according to our previous results. We then investigated the characteristics of the cavitation intensity of the M-H valve and S-B valve by means of a synchronized analysis of the visual images of cavitation and the pressure signals using our pneumatic ventricular assist device.

Materials and methods

The PVAD used was developed by the National Cardiovascular Center in Japan (Fig. 1). It has an outer diameter of 88 mm, a depth of 47 mm, and a stroke volume of 75 ml.[16] A 23-mm M-H valve (Medtronic, Minneapolis, MN, USA) and a 23-mm S-B valve (Sorin Biomedica, Vercelli, Italy) were mounted in the inlet valve port after the sewing rings were removed (Fig. 2). For the inlet valve, the major orifice direction of the monoleaflet valve and the leaflet tip direction of the bileaflet valve were set at a 45° clockwise orientation. In contrast, for the outlet valve, these angles were set at a 45° counterclockwise orientation (Fig. 3).

Even though the outer ring diameter of the S-B valve is smaller than that of the M-H valve, the orifice diameter of the S-B valve is larger that that of the M-H valve (Table 1). The PVAD was operated at a positive pressure of 220 mmHg and a negative pressure of –60 mmHg using a control – drive console for circulatory support (VCT-30; Toyobo, Osaka, Japan). The PVAD was connected to a Donovan mock circulatory loop tester and was run at heart rates of 70 beats/min with a systolic ratio of 43% and a bypass flow of 5.0 l/min.

To perform a synchronized analysis of the images of cavitation and the pressure signal of cavitation bubble collapse, we employed a function generator to provide a square pulse, which was used as a trigger signal for the ECG-R mode of the control – drive console for circulatory support (Fig. 4). This square pulse was delayed by a delay circuit and used as the trigger signal for a pressure sensor and a high-speed video camera (Fig. 4). The mean aortic

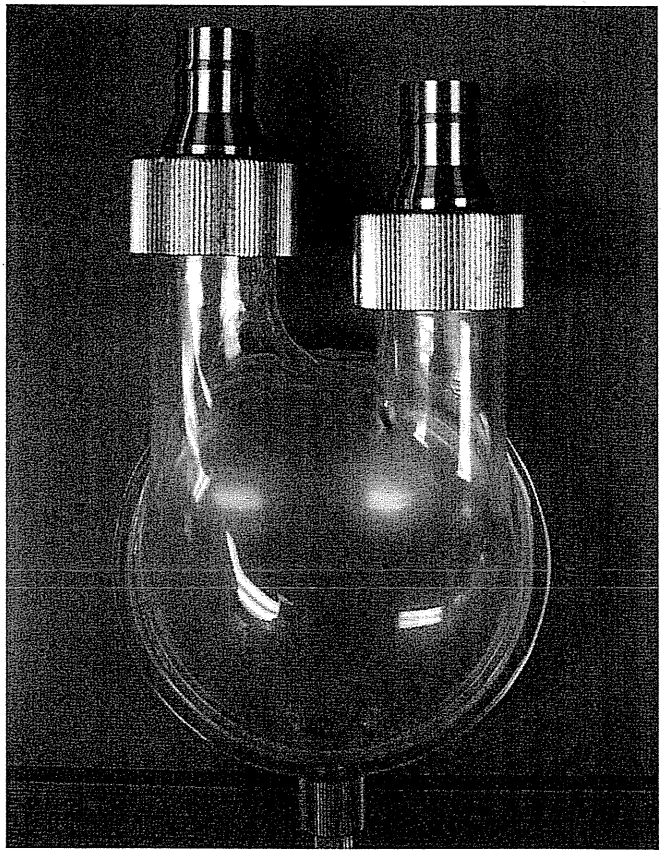

Fig. 1. Photograph of the pneumatic ventricular assist device (VAD) developed by our group. It has an outer diameter of 88 mm, a depth of 47 mm, and a stroke volume of 75 ml

Table 1. Configurations of the Medtronic Hall valve and the Sorin Bicarbon valve

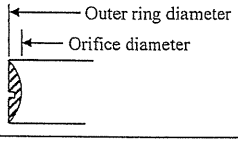

Valves	Sewing ring diameter (mm)	Outer ring diameter (mm)	Orifice diameter (mm)	Orifice area (cm^2)	Opening angle
M-H valve	23	19.4	18.0	2.54	70°
S-B valve	23	19.2	18.7	2.8	60°

M-H, Medtronic Hall; S-B, Sorin Bicarbon

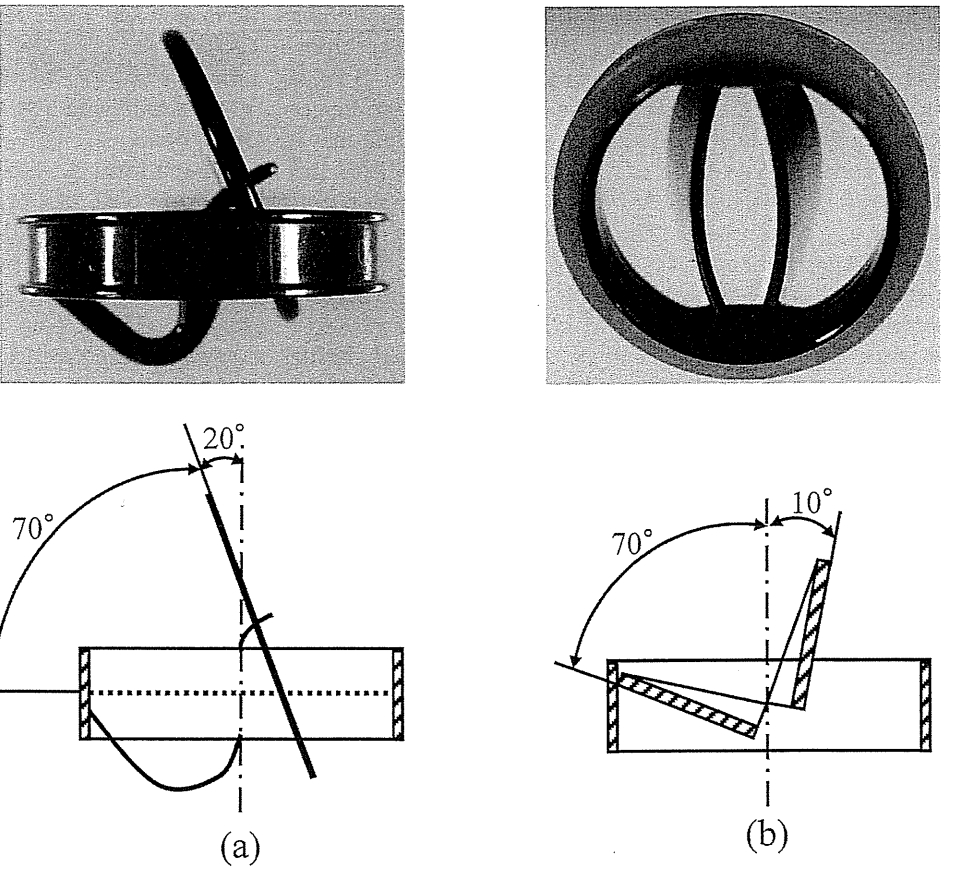

Fig. 2. Photographs and opening angles of the mechanical heart valves studied: **a** Medtronic Hall (M-H) valve and **b** the Sorin Bicarbon (S-B) valve

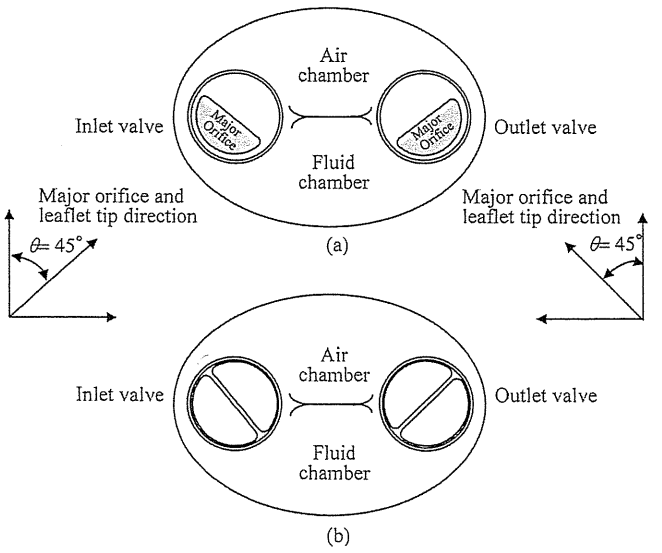

Fig. 3. Valve orientation angles for the M-H valve (**a**) and the S-B valve (**b**). This illustration shows the top view of the pneumatic VAD

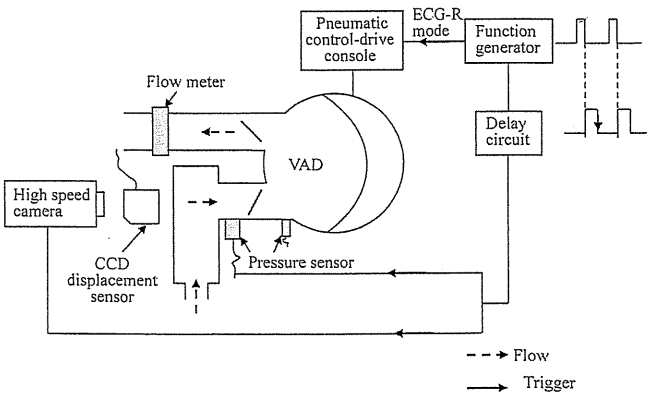

Fig. 4. Diagram of the synchronized experimental system. A function generator was employed to provide a square pulse and an Electrocardiogram R wave (*ECG-R*) mode trigger signal for the control – drive console. In addition, this square pulse was delayed by a delay circuit and used as the trigger signal for one of the pressure sensors and the high-speed video camera. *CCD*, charge-coupled device

and atrial pressures were maintained at 100 mmHg and 7 mmHg, respectively. The blood analog fluid was a mixture of 50% water and 50% glycerol by volume, which had a viscosity coefficient of 3.4 cP, a density of 1.12 g/cm^3, and a vapor pressure of –715 mmHg at 37°C.

A charge-coupled device (CCD) laser displacement sensor (LC-2450; Keyence, Osaka, Japan) with a sampling frequency of 50 kHz was used to detect the valve-closing motion (Fig. 4). The chamber was constructed of acrylic resin for optical access, and the laser displacement sensor was placed on top of the acrylic chamber (Fig. 4). A high-speed camera (Memrecam fx-6000; Nac Image, Tokyo, Japan) was also placed on top of the acrylic chamber and images of the cavitation bubbles were recorded at 30 000 frames/s. A miniature absolute pressure sensor (105C02;

PCB Piezotronics, Depew, NY, USA) with a resonant frequency of 250 kHz was mounted 10 mm away from the inlet valve surface. The data were stored using a digital oscilloscope (DL1640L; Yokogawa, Tokyo, Japan) at a 1-MHz sampling rate. The driving pressure and ventricular pressure of the PVAD were measured by a pressure transducer (MP5100; Baxter, Deerfield, IL, USA) with a sampling frequency of 1 kHz. The pressure signal was band-pass filtered between 35 and 200 kHz using a digital filter (Labview 7.0; National Instruments, Austin, TX, USA).

Results

The flow, aortic pressure, left atrial pressure, ventricular pressure (equal to the pump internal pressure), and the driving pressure wave are shown in Fig. 5. These pressures were set at the same level as those in humans. The ventricular pressure reached levels above 200 mmHg after valve closure (Fig. 5d).

The pressure signal near the valve surface and the valve-closing motion are shown in Fig. 6. The pressure signal dropped before the valve was completely closed (Fig. 6), and this result was attributed to squeeze flow. The pressure drop after valve closure was caused by the water hammer effect. In the case of the S-B valve, there were two negative peak pressures. The first negative peak pressure (point A of Fig. 6b) occurred when the right leaflet closed, and the second negative peak pressure (point B of Fig. 6b) occurred when the left leaflet closed. A rebound motion of the leaflet was observed for the S-B valve (point C of Fig. 6b); however, there was no rebound motion in the M-H valve.

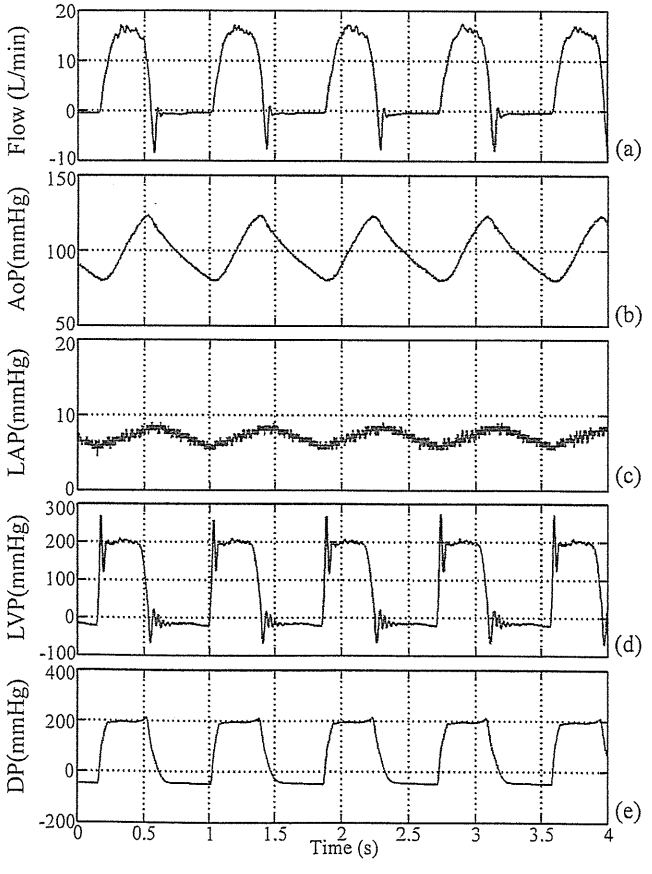

Fig. 5. Pressure signal at the M-H valve for a heart rate of 70 beats/min. *a* Flow rate, *b* aortic pressure (*AoP*), *c* left atrial pressure (*LAP*), *d* left ventricular pressure (*LVP*, equal to the pump internal pressure), and *e* driving air pressure (*DP*)

Synchronized results of the cavitation images and pressure signals near the valve surface are shown in Figs. 7, 8. Point A of Fig. 7a is the point at which the valve closes. For the M-H valve, the cavitation bubbles occurred just before the valve closed (dots inside the circle of Fig. 7c). The cavitation bubbles were concentrated near the valve stop, and were observed for 267 μs. The S-B valve (Fig. 8) has two leaflets, and thus the valve-closing motion is complicated. Point A of Fig. 8a is the point where the left leaflet closes first, and point B is where the right leaflet closes second. Cavitation bubbles were observed when the right leaflet closed in the S-B valve. Cavitation bubbles associated with the S-B valve were concentrated at the tip of the leaflet and were observed for 100 μs (dots inside the circle of Fig. 8c). The visual cavitation time of the S-B valve was shorter than that of the M-H valve. The data for the M-H valve and the S-B valve are shown in Table 2. The RMS pressures at the M-H valve and the S-B valve were 19.6 and 11.7 mmHg, respectively, after the pressure signal was band-pass filtered. Moreover, the valve-closing velocity of the M-H valve was faster than that of the S-B valve.

Discussion

Currently, both the visual cavitation time[6,9,15] and the root mean square (RMS)[7–9] value of the pressure were used to evaluate the cavitation intensity of a MHV. The visual cavitation time can be calculated by the Rayleigh analysis for a spherical cavity in a inviscid incompressible liquid:[2]

$$t_{visual\ time} = 0.951 R_{\max} \sqrt{\frac{\rho}{p_\infty}} \quad (1)$$

where ρ is the density of the liquid, $R_{\max}$ is the maximum radius of the cavitation bubble, and p_∞ is the pressure at infinity. As shown in Eq. 1, the visual cavitation time depends on the size of the cavitation bubbles. The peak pressure when a collapse of cavitation bubbles occurs is given roughly by the following:[2]

$$P_{\max} \approx 100 R_{\max} \frac{p_\infty}{r} \quad (2)$$

where r is the distance from the bubble center. As shown in Eq. 2, high pressure is generated when large cavitation bubbles collapse. In particular, a high pressure of about 1 GPa is generated near the center of the bubbles. As shown in Fig. 7, the diameter of the spherical cavitation bubbles

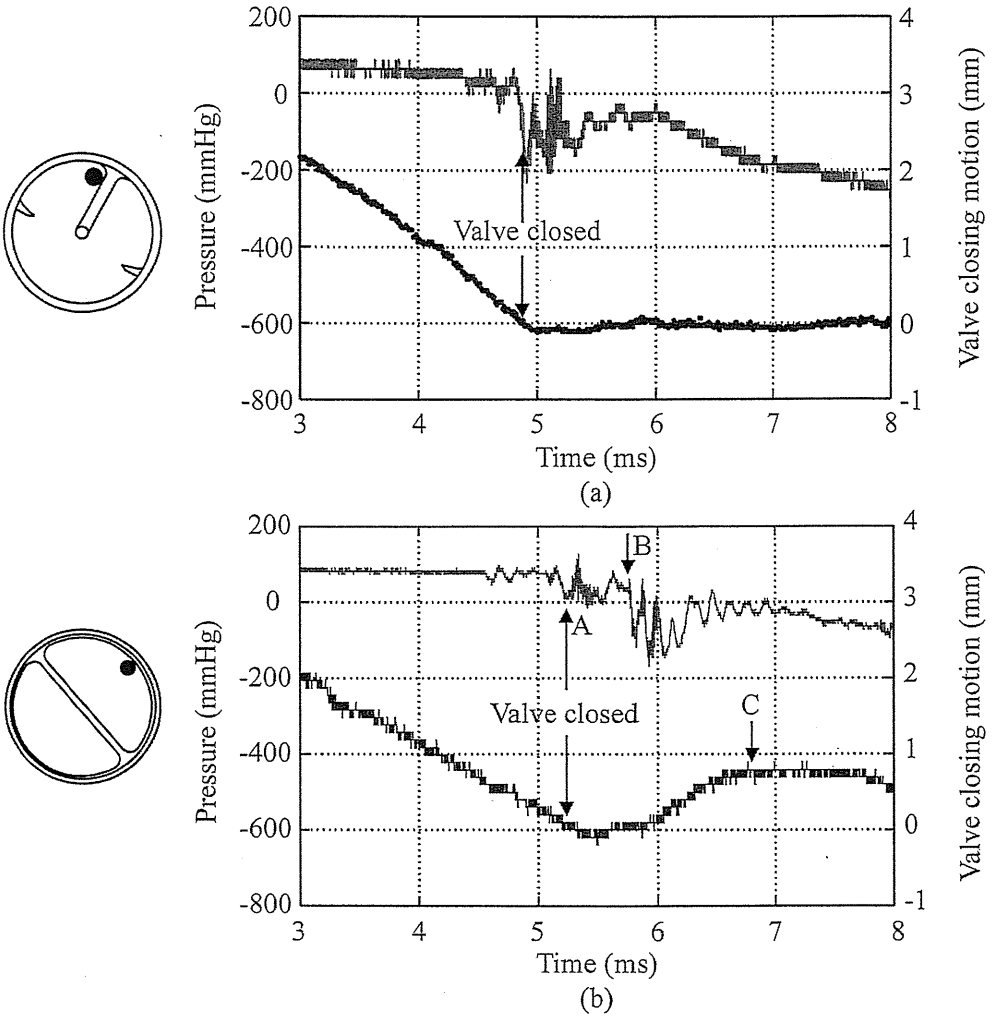

Fig. 6. Pressure signal near the leaflet surface (*upper line*) and the valve-closing motion (*lower line*) at a heart rate of 70 beats/min for the M-H valve (**a**) and the S-B valve (**b**). *A*, right side leaflet closure; *B*, left side leaflet closure; *C*, rebound motion of the leaflet. *solid circle*, location at which the valve motion and pressure were measured

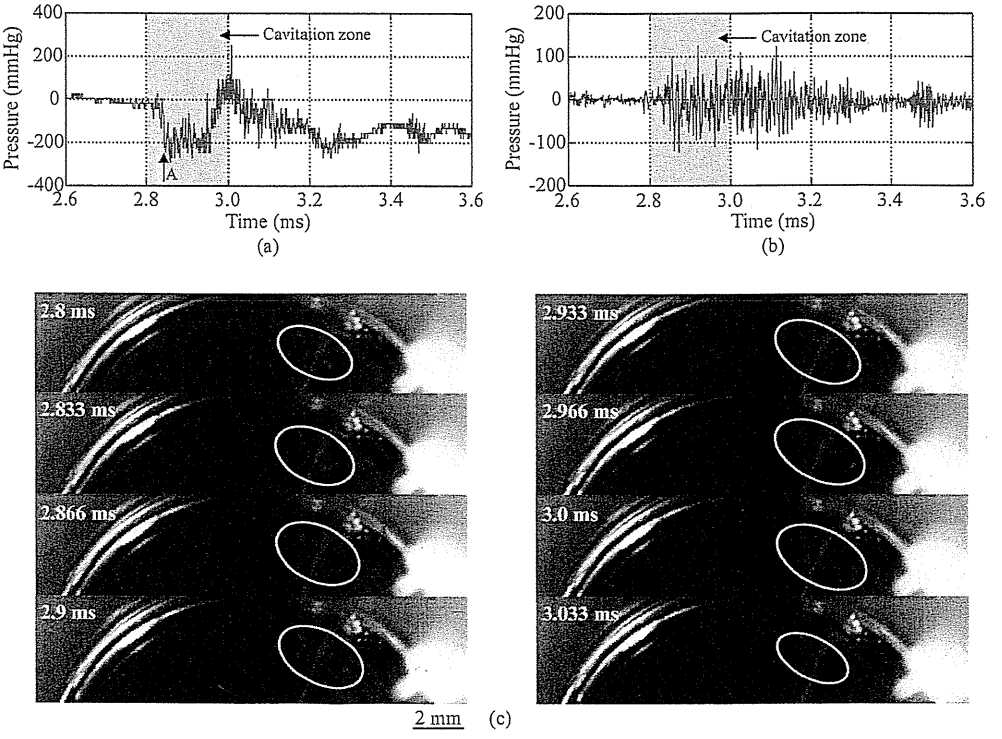

Fig. 7a–c. Synchronized results of the cavitation bubbles and pressure signal for the M-H valve at a heart rate of 70 beats/min. **a** Pressure signal before band-pass filtering and **b** after band-pass filtering between 35 and 200 kHz. **c** Cavitation bubbles (*circled*) recorded using a high-speed camera at 30000 frames/s. *A*, leaflet closure

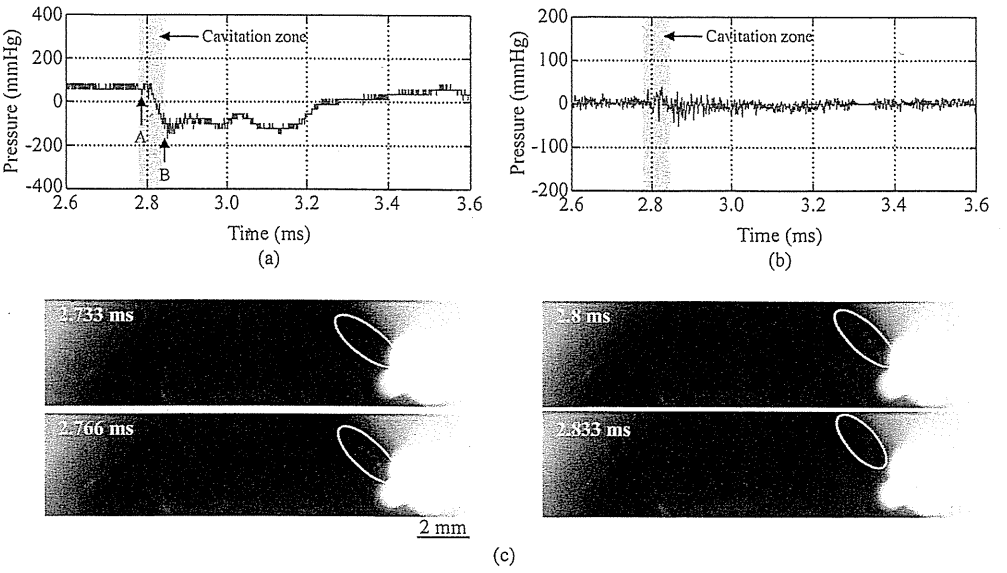

Fig. 8a–c. Synchronized results of the cavitation bubbles and pressure signal for the S-B valve at a heart rate of 70 beats/min. **a** Pressure signal before band-pass filtering and **b** after band-pass filtering between 35 and 200 kHz. **c** Cavitation bubbles (*circled*) recorded using a high-speed camera at 30000 frames/s. *A*, right side leaflet closure, *B*, left side leaflet closure

Table 2. Valve-closing velocity, cavitation time, and pressure for the two valves studied

Valve	Closing velocity (m/s)	Visual cavitation time (μs)	RMS pressure (mmHg)
Medtronic Hall valve	1.2 ± 0.25	255 ± 30.5	19.6 ± 3.1
Sorin Bicarbon valve	0.85 ± 0.15	100.2 ± 26.2	11.7 ± 2.4
Medtronic valve/Sorin valve	1.41	2.54	1.67

The valve-closing velocity was calculated from the valve-closing motion of Fig. 5 at 0.5 ms before valve closure
RMS, root mean square

generated by the S-B valve was about 0.3 mm. From Eq. 1, we can calculate the theoretical visual cavitation time as 145 μs. In this study, we could find cavitation bubbles with a maximum diameter of about 0.3 mm (Figs. 7 and 8), and observed the cavitation bubbles for 100–250 μs. This means that the experimental results of this study are consistent with the theoretical results of Eq. 1. The peak pressure at the bubble wall calculated using Eq. 2 is 10 MPa when this size of cavitation bubble collapses. This is high enough to damage red blood cells.[4]

Cloud cavitation was observed at the M-H valve (Fig. 7c). The size of the cloud cavitation was not measured, but it was generated at high fluid velocity, and then a high pressure of more than 200 MPa resulted when the cloud cavitation collapsed.[2] In general, the pressure generated by the collapse of cloud cavitation is higher than that generated by the collapse of spherical cavitation bubbles,[2] resulting in severe erosion pitting and blood cell trauma.[4] As shown in Figs. 7 and 8, we observed the visual cavitation time and the timing of the generation and collapse of cavitation bubbles from the images of cavitation. Moreover, we were able to estimate the theoretical magnitude of the pressure at the collapse of the cavitation bubbles; however, we could not measure the real magnitude of the pressure when large cavitation bubbles collapsed.

The RMS pressure is a statistical measure of the magnitude of a varying quantity, and can be written as:

$$P_{RMS} = \sqrt{\frac{1}{T_2 - T_1}\int_{T_1}^{T_2} [P(t)]^2\, dt}, \qquad T_1 \le t \le T_2 \tag{3}$$

where, $P(t)$ is the fluctuating pressure. In general, MHVs have a wide range of pressure frequencies.[17] In a previous study, we carried out a frequency analysis using the M-H valve and found that the pressure frequency caused by contact with the valve housing ranged from 1–30 kHz.[18] Therefore, the band-pass filtered pressure signal from 35 to 200 kHz was associated with the collapse of cavitation bubbles. As shown in Eq. 3, the RMS pressure after the pressure signal was band-pass filtered shows the fluctuating pressure caused by the collapse of the cavitation bubbles, and this reflects the magnitude of cavitation intensity. A high-frequency signal was also observed after the collapse of the cavitation bubbles. In this study, we recorded the cavitation images at the valve stop of the M-H valve and at the tip of the right leaflet of the S-B valve only. However, there is a possibility for cavitation bubbles to occur at the center hole and at the inner side of the M-H valve as a result of the venturi effect and the water hammer effect. With the S-B valve, there is also a possibility for cavitation bubbles to occur at the tip of the left leaflet. However, a high-frequency pressure signal might occur due to squeeze flow at the clearance after the valve completely closes. The RMS pressure is indistinguishable from the pressure signal cause of cavitation bubble collapse to cause of valve contact

noise,[19] but it could define the magnitude of the pressure caused by the collapse of different sizes of cavitation bubble.

In this study, the RMS pressure of the M-H valve was 1.67 times that of the S-B valve. In addition, the visual cavitation time of the M-H valve was 2.54 times that of the S-B valve. As shown in Figs. 7 and 8, the size and area of cavitation bubbles formed at the M-H valve was about five times those at the S-B valve. Based on this fact, it is very likely that not only the visual cavitation time, but also the RMS pressure, could be used as a measure of the MHV cavitation intensity in an artificial heart.

Even though the outer ring diameter of the S-B valve is smaller than that of the M-H valve, the orifice diameter of the S-B valve is larger that that of the M-H valve (Table 1). This means that the characteristics of the flow dynamics of the S-B valve are superior to those of the M-H valve. Also, the cavitation intensity of the S-B valve is less than that of the M-H valve. This result has led us to the following hypothesis: the S-B valve may cause less blood cell damage than the M-H valve does. In a previous study, we reported that the inlet valve orientation angle of the M-H valve in the PVAD affected the flow pattern inside the pump;[16] however, we do not yet have results for the S-B valve. In the future, we will investigate the washout effect inside the PVAD with the S-B valve, and if the washout effect is good, we will use the S-B valve in the PVAD.

Conclusions

We investigated the characteristics of the cavitation intensity by performing synchronized analysis of the cavitation images and pressure signals of cavitation bubble collapse in a PVAD. The RMS pressure is indistinguishable from the pressure signal of cause cavitation bubble collapse to cause of valve contact noise; however, the magnitude of the pressure is determined by the collapse of the cavitation bubbles. Both the visual cavitation time and the RMS pressure characterize the cavitation intensity, and this is a very important factor when estimating MHV cavitation intensity in an artificial heart.

Acknowledgments This work was supported by the Program for the Promotion of Fundamental Studies in Health Science of the National Institute of Biomedical Innovation (NIBIO) and by a Grant-in-Aid for Scientific Research from the Japan Society for the Promotion of Science (JSPS) (No. 19650120).

References

1. Yoganathan AP, Chandran KB, Sotiropoulos F. Flow in prosthetic heart valves: state-of-the-art and future directions. Ann Biomed Eng 2005;33(12):1689–1694
2. Knapp RT, Daily JW, Hammitt FG. Cavitation. Iowa City: Institute of Hydraulic Research, University of Iowa, 1979
3. Brennen CE. Cavitation and bubble dynamics. New York: Oxford University Press, 1995
4. Grigioni M, Daniele C, D'Avenio G, Barbaro V. A discussion on the threshold limit for hemolysis related to Reynolds shear stress. J Biomech 1999;32:1107–1112
5. Klepetko W, Moritz A, Mlczoch J, Schurawitzki H, Domanig E, Wolner E. Leaflet fracture in Edward-Duromedics bileaflet valves. J Thorac Cardiovasc Surg 1989;97:90–94
6. Lee HS, Tsukiya T, Homma A, Kamimura T, Takewa Y, Tatsumi E, Taenaka Y, Takano H, Kitamura S. Observation of cavitation bubbles in monoleaflet mechanical heart valves. J Artif Organs 2004;7:121–127
7. Potthast K, Erdönmen G, Schnelke C, Sellin L, Sliwka U, Schöndube F, Eichler M, Reul H. Origin and appearance of HITS induced by prosthetic heart valves: an in vitro study. Int J Artif Organs 2000;23:441–445
8. Wu C, Liu JS, Hwang NHC, Lin YKM. Statistical correlation between transient pressure drop and cavitation at closure of a mechanical heart valve. ASAIO J 2005;51:11–16
9. Lukic B, Zapanta CM, Griffith KA, Weiss WJ. Effect of the diastolic and systolic duration on valve cavitation in a pediatric pulsatile ventricular assist device. ASAIO J 2005;51:546–550
10. Biancucci BA, Deutsch S, Geselowitz DB, Tarbell JM. In vitro studies of gas bubble formation by mechanical heart valves. J Heart Valve Dis 1999;8:186–196
11. Wu C, Herman BA, Retta SM, Grossman LW, Liu JS, Hwang NHC. On the closing sounds of a mechanical heart valve. Ann Biomed Eng 2005;33(6):743–750
12. Sneckenberger DS, Stinebring DR, Deutsch S, Geselowitz DB, Tarbell JM. Mitral heart valve cavitation in an artificial heart environment. J Heart Valve Dis 1996;5:216–227
13. Sohn K, Manning KB, Fontaine AA, Tarbell JM, Deutsch S. Acoustic and visual characteristic of cavitation induced by mechanical heart valves. J Heart Valve Dis 2005;14:551–558
14. Ritchie RO. Fatigue and fracture of pyrolytic carbon: a damage-tolerant approach to structural integrity and life prediction in ceramic heart valve prostheses. J Heart Valve Dis 1996;5(Suppl I): S9–S31
15. Lee HS, Homma A, Taenaka Y. Hydrodynamic characteristics of bileaflet mechanical heart valves in an artificial heart: cavitation and closing velocity. Artif Organs 2007;31(7):532–537
16. Akagawa E, Lee HS, Tatsumi E, Homma A, Tsukiya T, Katagiri N, Kakuta Y, Nishinaka T, Mizuno T, Ota K, Kansaku R, Taenaka Y. Effects of mechanical valve orifice direction on flow pattern in a ventricular assist device. J Artif Organs 2007;10:85–91
17. Johansen P. Mechanical heart valve cavitation. Expert Rev Med Devices 2004;1(1):95–104
18. Lee HS, Tatsumi E, Taenaka Y. Effect of systolic duration on mechanical heart valve cavitation in a pneumatic ventricular assist device: using a monoleaflet valve. ASAIO J 2008;54(1):25–30
19. Herbertson LH, Reddy V, Manning KB, Welz JP, Fontaine AA, Deutsch S. Wavelet transforms in the analysis of mechanical heart valve cavitation. J Biomech Eng 2006;128:217–222

Artificial Organs
32(6):453–460, Blackwell Publishing, Inc.

Characteristics of Mechanical Heart Valve Cavitation in a Pneumatic Ventricular Assist Device

Hwansung Lee and Yoshiyuki Taenaka

Department of Artificial Organs, Research Institute, National Cardiovascular Center, Osaka, Japan

Abstract: In previous studies, we investigated the mechanism of mechanical heart valve (MHV) cavitation and cavitation intensity with a nonsynchronized experiment system. Our group is currently developing a pneumatic ventricular assist device (PVAD), and in this study we investigated MHV cavitation intensity in the PVAD using a synchronized analysis of the cavitation images and the acoustic signal of cavitation bubbles. A 23-mm Medtronic Hall valve with an opening angle of 70° was mounted in the mitral position of the PVAD after removing the sewing ring. A function generator provided a square signal, which used the trigger signal of the electrocardiogram R wave (ECG-R) mode of the control-drive console for circulatory support. This square signal was delayed by a delay circuit and was then used as the trigger signal for a pressure sensor and a high-speed video camera. The data were stored using a digital oscilloscope at a 1-MHz sampling rate, and then the pressure signal was band-pass filtered between 35 and 200 kHz using a digital filter. The band-pass filtered root mean squared (RMS) pressure and cavitation cycle duration were used as an index of cavitation intensity. The cavitation bubbles were concentrated at the valve stop, and the cavitation cycle duration and RMS pressure increased as the heart rate and driving pressure increased. At the low valve-closing velocity, bubble cavitation was observed near the valve stop. However, at the fast valve-closing velocity, cloud cavitation was observed. A high-frequency signal wave was generated when the bubbles collapsed. The cavitation cycle duration and RMS pressure increased as the valve-closing velocity increased linearly. **Key Words:** Pneumatic ventricular assist device—Mechanical heart valve—Cavitation.

Cavitation is the rapid formation and collapse of vapor-filled cavities that occurs when a fluid is exposed to rapid changes in pressure below liquid vapor pressure (1,2). When cavitation occurs near the material surface of a mechanical heart valve (MHV), this rapid collapse may cause the generation of a high-speed micro-jet and shock waves, resulting in the generation of high pressure. Kornberg et al. observed leaflet escape due to a strut fracture at 42 months after implantation of a monoleaflet MHV (3). Klepetko et al. observed microscopic pitting on a bileaflet valve at 36 and 38 months after implantation (4). Those pyrolytic carbon fractures appeared to be primarily the result of the cavitation phenomenon.

doi:10.1111/j.1525-1594.2008.00564.x

Received April 2007; revised August 2007.

Address correspondence and reprint requests to Dr. Hwansung Lee, Department of Artificial Organs, The Advanced Medical Engineering Center, Research Institute, National Cardiovascular Center, 5-7-1, Fujishiro-dai, Suita, Osaka 565-8565, Japan. E-mail: hslee@ri.ncvc.go.jp

In our previous studies, we investigated MHV cavitation in an electro-hydraulic total artificial heart (EHTAH) (5–7). We reported that most of the cavitation bubbles were observed around the valve stop and were caused by the squeeze flow, and the formation of cavitation bubbles depended on the valve-closing velocity and valve leaflet geometry (5–7).

As it relates to squeeze flow, the observation time of the cavitation bubbles (herein, the cavitation cycle duration) is closely related to the valve-closing velocity, and hence the cavitation cycle duration is a valid parameter for determining the MHV cavitation intensity. However, this method does not account for the size of cavitation bubbles. Other research groups have suggested that high-intensity transient pressure detected by ultrasonography was useful as an indication of cavitation intensity (8–12). The frequency of the pressure signal when cavitation bubbles collapse has been investigated using a pressure sensor or hydrophone, but the results varied widely (13–15). However, these experiments were performed under nonsynchronized conditions between the visual

observation of cavitation and the emitting of an acoustic signal. Sohn et al. achieved synchronization between the visual images and acoustic signals, and reported that the growth and collapse of cavitation bubbles was correlated with a specific acoustic signature (16). However, his group used a nonpulsatile device, and the cavitation cycle duration they recorded was longer than those recorded in our previous results. The different driving mechanism might have caused the difference in MHV cavitation intensity.

In our laboratory, we have been developing a diaphragm-type pneumatic ventricular assist device (PVAD). The hydrodynamic characteristics of the bileaflet valve have proven superior to those of monoleaflet valves, and thus the majority of MHVs currently in clinical use are bileaflet valves. Most of the valve housing of a bileaflet valve is made of pyrolytic carbon. The MHVs are mounted on a rigid mounting structure by insertion of a blood pump port made of polyurethane, after removing the MHV sewing ring. If compressive stress acts upon the valve housing made of pyrolytic carbon, the opening and closing motion of the leaflet might be disturbed. For this reason, bileaflet valves have not been used in our artificial heart. The Medtronic Hall valve (Medtronic, Inc., Minneapolis, MN, USA) has excellent durability, very good hemodynamic performance, and exceptionally low thrombogenicity, leading to good long-term survival with low complication rates (17). In addition, we assumed that the flow through the major orifice of the monoleaflet valve acted on the blood pump in some way, which is good for the washout effect inside the blood pump, resulting in the prevention of thrombosis. For these reasons, we incorporated the Medtronic Hall monoleaflet valve in an EHTAH and the PVAD. We examined the cavitation intensity of the Medtronic Hall valve in an EHTAH in several studies (5–7). However, the geometry of the blood pump and driving mechanism were significantly different between the EHTAH and the PVAD. The MHV cavitation intensity may differ in response to the geometry of the blood pump and driving mechanism. In this study, we investigated the cavitation intensity of the monoleaflet valve. We also attempted to perform a synchronized analysis between the visual images of cavitation and acoustic signals using the PVAD.

MATERIALS AND METHODS

A diaphragm-type PVAD was developed by the National Cardiovascular Center in Japan (Fig. 1). It has an outer diameter of 88 mm, a thickness of 47 mm, and a stroke volume of 75 mL (18). A 23-mm Medtronic Hall valve (Medtronic, Inc.) with an opening angle of 70° was mounted in the mitral position after removing the sewing ring. The PVAD was connected to a Donovan mock circulatory loop tester. It consists of four chambers: the right atrium chamber, pulmonary arterial chamber, left atrium chamber, and arterial chamber. The compliance of each chamber is determined by the volume of air trapped above the fluid in that chamber. Our PVAD was operated at a positive pressure ranging from 200 to 250 mm Hg and a negative pressure ranging from –50 to –85 mm Hg with a control-drive console for circulatory support (VCT-30; Toyobo, Osaka, Japan). The PVAD was run at heart rates ranging from 60 to 90 bpm and cardiac output ranging from 4.5 to 6.7 L/min.

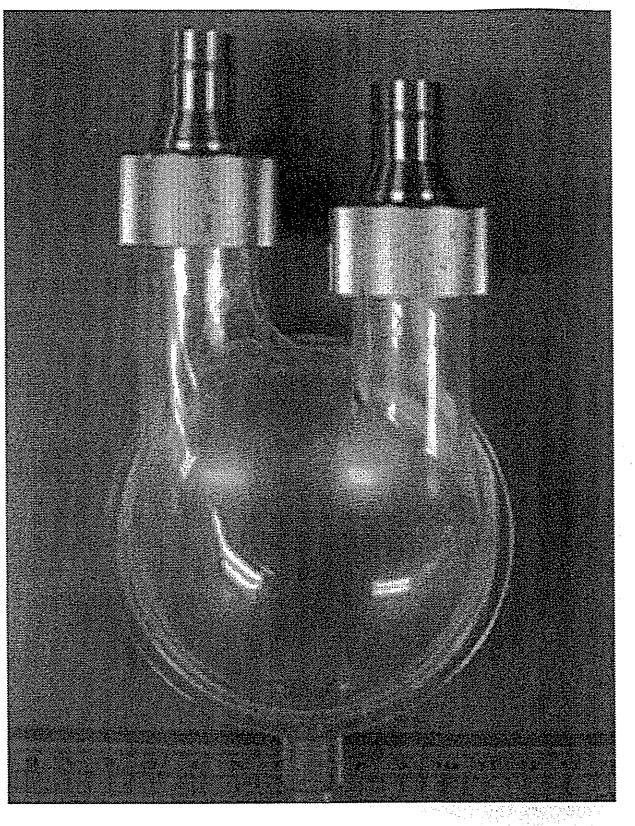

FIG. 1. Photograph of the pneumatic ventricular assist device.

To perform a synchronized analysis of the acoustic signal and the images of cavitation, we employed a function generator to provide a square signal, which used the trigger signal of the ECG-R mode of the control-drive console for circulatory support (Fig. 2). This square signal was delayed by a delay circuit and was then used as the trigger signal for a pressure sensor and a high-speed video camera (Fig. 2). The

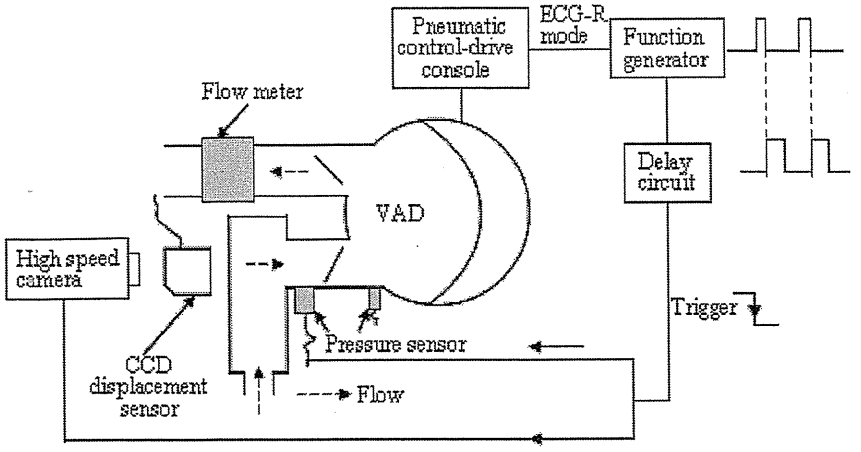

FIG. 2. Diagram of the synchronized experimental system.

mean aortic and atrial pressures were maintained at 100 mm Hg and 7 mm Hg, respectively. The blood analogue fluid was a mixture of 50% water and 50% glycerol by volume, which has a viscosity coefficient of 3.4 cP, a density of 1.12 g/cm^3, and a vapor pressure of –715 mm Hg at 37°C.

A closed circuit digital laser displacement sensor (LC-2450; Keyence, Osaka, Japan) with a sampling frequency of 50 kHz was used to detect the valve-closing motion (Fig. 2). The chamber was constructed of acrylic resin for optical access, and the laser displacement sensor was placed on top of the acrylic chamber (Fig. 2). A high-speed camera (Memrecam fx-6000; Nac Image Technology, Tokyo, Japan) was also placed on top of the acrylic chamber, and images of the cavitation bubbles were recorded at 30 000 frames per second. A miniature pressure sensor (105C02; PCB Piezotronics, Depew, NY, USA) with a resonance frequency of 250 kHz was mounted 10 mm away from the valve surface. The data were stored using a digital oscilloscope (DL1640 L; Yokogawa, Tokyo, Japan) at a 1-MHz sampling rate. The driving pressure and ventricular pressure of the PVAD were measured by a pressure transducer (MP5100; Baxter, Deerfield, IL, USA) with a sampling frequency of 1 kHz. The pressure signal was band-pass filtered between 35 and 200 kHz using a digital filter (Labview 7.0; National Instruments, Austin, TX, USA).

RESULTS

The driving pressure, ventricular pressure (equal to the pressure inside the pump), flow wave, and valve motion are shown in Fig. 3. The ventricular pressure reached the peak value, which was above 200 mm Hg, and the outlet valve opened before the inlet valve closed.

The pressure wave near the valve surface decreased before the valve was completely closed

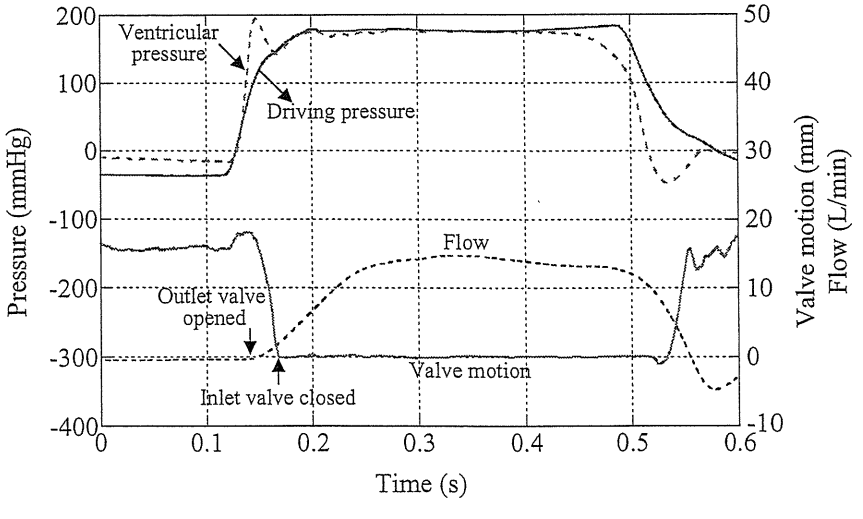

FIG. 3. Pressure–waves, flow rate, and valve motion at a heart rate of 70 bpm.

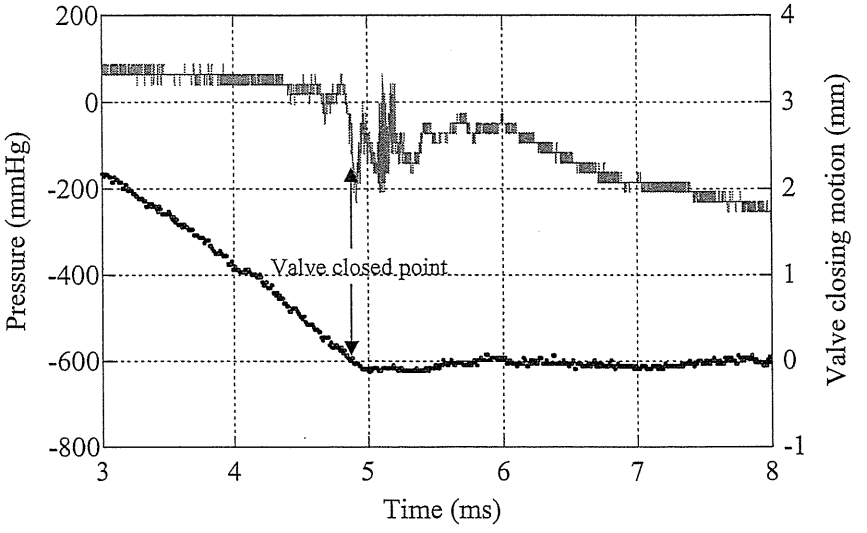

FIG. 4. Pressure signal near the leaflet surface and the valve-closing motion at a heart rate of 70 bpm.

(Fig. 4), and this result was attributed to squeeze flow. The higher-frequency pressure waves occurred after the valve closed. The valve-closing velocity during the 5 ms just before valve closure is shown in Fig. 5. The valve-closing velocity increased as the heart rate and driving pressure increased, and the velocity ranged from 0.76 ± 0.12 to 1.16 ± 0.13 m/s (Fig. 5).

The synchronization between the cavitation images and pressure signals near the valve surface are shown in Figs. 6 and 7. At a heart rate of 60 bpm, the cavitation bubbles were generated after the valve was completely closed (Fig. 6a). A peak pressure wave was generated by the collapse of the cavitation bubbles (Fig. 6b). The cavitation bubbles generated at valve closure were observed during the 0.1 ms before the valve closed (Fig. 6c). At a heart rate of 90 bpm, cavitation bubbles were generated before the valve closed completely (Fig. 7a), and they then became cloud cavitation. Strong pressure waves were generated by cavitation bubbles' collapse (Fig. 7b). This cloud cavitation was observed for 0.3 ms (Fig. 7c).

The cavitation cycle duration ranged from 100 ± 29.3 to 287.6 ± 26.7 μs and increased as the heart rate increased (Fig. 8). The root mean squared (RMS) pressure ranged from 12.0 ± 1.7 to 22.1 ± 2.5 mm Hg and also increased as the heart rate increased (Fig. 9).

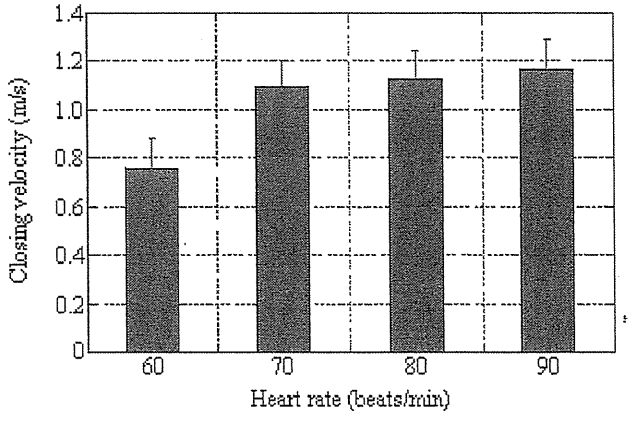

FIG. 5. Valve-closing velocity. This is the average velocity during the 5 ms just before valve closure.

DISCUSSION

In this study, we performed a synchronized analysis between cavitation images and the cavitation acoustic signal using a PVAD. We were able to observe a high-frequency signal during cavitation (Figs. 6 and 7). In previous studies, we estimated the MHV cavitation intensity using the cavitation cycle duration only (6,7). However, this method did not account for the size of cavitation bubbles. When cavitation bubbles are large, the cavitation cycle duration is longer. In the case of many small bubbles, even if the duration of the cavitation cycle is short, the cavitation intensity might be strong. Other groups have estimated the MHV cavitation intensity using the band-pass filtered RMS pressure and the high-intensity transient signals (9–11,15,19). However, the pressure signals varied depending on the kinds of MHV cavitation.

The fluid in the gap space between the leaflet and the valve stop was squeezed into motion during the valve-closing phase, creating squeeze flow during the final period of valve closure. Cavitation bubbles were generated before leaflet contact with the valve stop

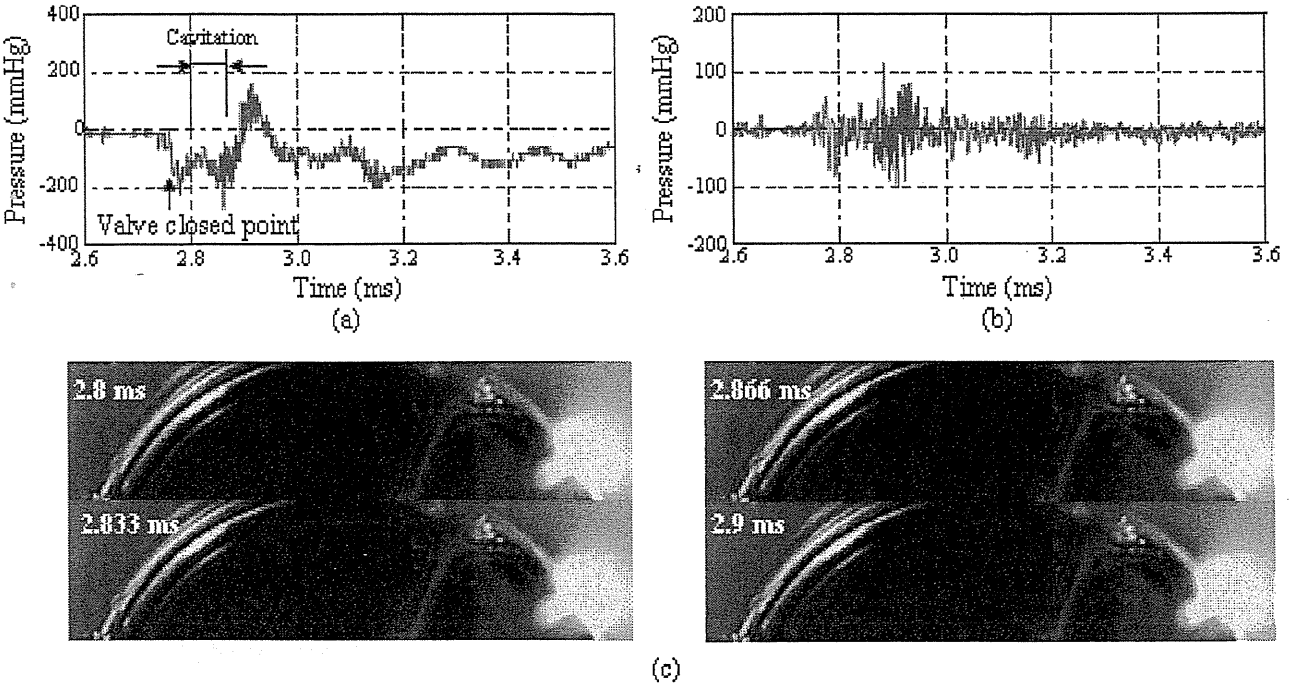

FIG. 6. Cavitation bubbles and pressure signal at a heart rate of 60 bpm. (a) Pressure signal; (b) Band-pass filtered signal; (c) Images of cavitation bubbles. The pressure signal was band-pass filtered between 35 and 200 kHz using a digital filter. Images of cavitation bubbles were taken with a high-speed camera at 30 000 frames per second.

(Figs. 6 and 7). At a low heart rate with slow valve-closing velocity (Fig. 6), the leaflet approach velocity to the valve stop was slow, and then cavitation bubbles were generated after the valve closed. In contrast, at a high heart rate with a fast valve-closing velocity (Fig. 7), the valve-approach velocity to the valve stop was fast, and then the fluid between the valve and valve stop was squeezed before the valve closed, generating cavitation bubbles before the valve closed.

This study clearly demonstrated that the mechanism for the MHV cavitation was dependent on the valve-closing velocity. In the case of low valve-closing velocity (Fig. 6), cavitation bubbles were generated, while cloud cavitation was observed at high valve-closing velocity (Fig. 7c). The collapse of a cloud of bubbles can cause more intense noise and more potential for damage than occurs with single-bubble cavitation (2). The high RMS pressure was caused by the cloud cavitation collapse (Fig. 7b). It is likely that the high valve-closing velocity caused severe damage to the valve surface and blood cell trauma. The RMS pressure at a heart rate of 90 bpm was 1.8 times larger than that at a heart rate of 60 bpm. On the other hand, the cavitation cycle duration at a heart rate of 90 bpm was 2.9 times as much as that at a heart rate of 60 bpm. As shown in Figs. 6–7, the size and area of cavitation bubbles at a heart rate of 90 bpm were more than three or four times larger than at a heart rate of 60 bpm. Based on this fact, it is very likely that not only the cavitation cycle duration but also the RMS pressure could be a measure of the MHV cavitation intensity in an artificial heart.

A high-frequency signal was also observed after the collapse of the cavitation bubbles. Cavitation bubbles caused by rebound were not observed during the experiment. We recorded the cavitation images on the valve stop only. However, the cavitation bubbles could be observed on the center hole, due to the venturi effect, and on the inner side of the valve surface, due to the water hammer effect (5). It was likely that the high-frequency signal after the collapse of the cavitation bubbles was caused by the collapse of cavitation bubbles at one of these locations.

The US Food and Drug Administration (FDA) has recommended calculating the transvalvular pressure difference (dP/dt) by a linear regression of the transvalvular pressure difference during the last 20 ms before closure when performing cavitation experiments (20). However, the dP/dt is the difference according to the aorta and ventricle compliance, and when five laboratories compared results according to the FDA guidelines, there were significant differences in the results (21). Our PVAD has no

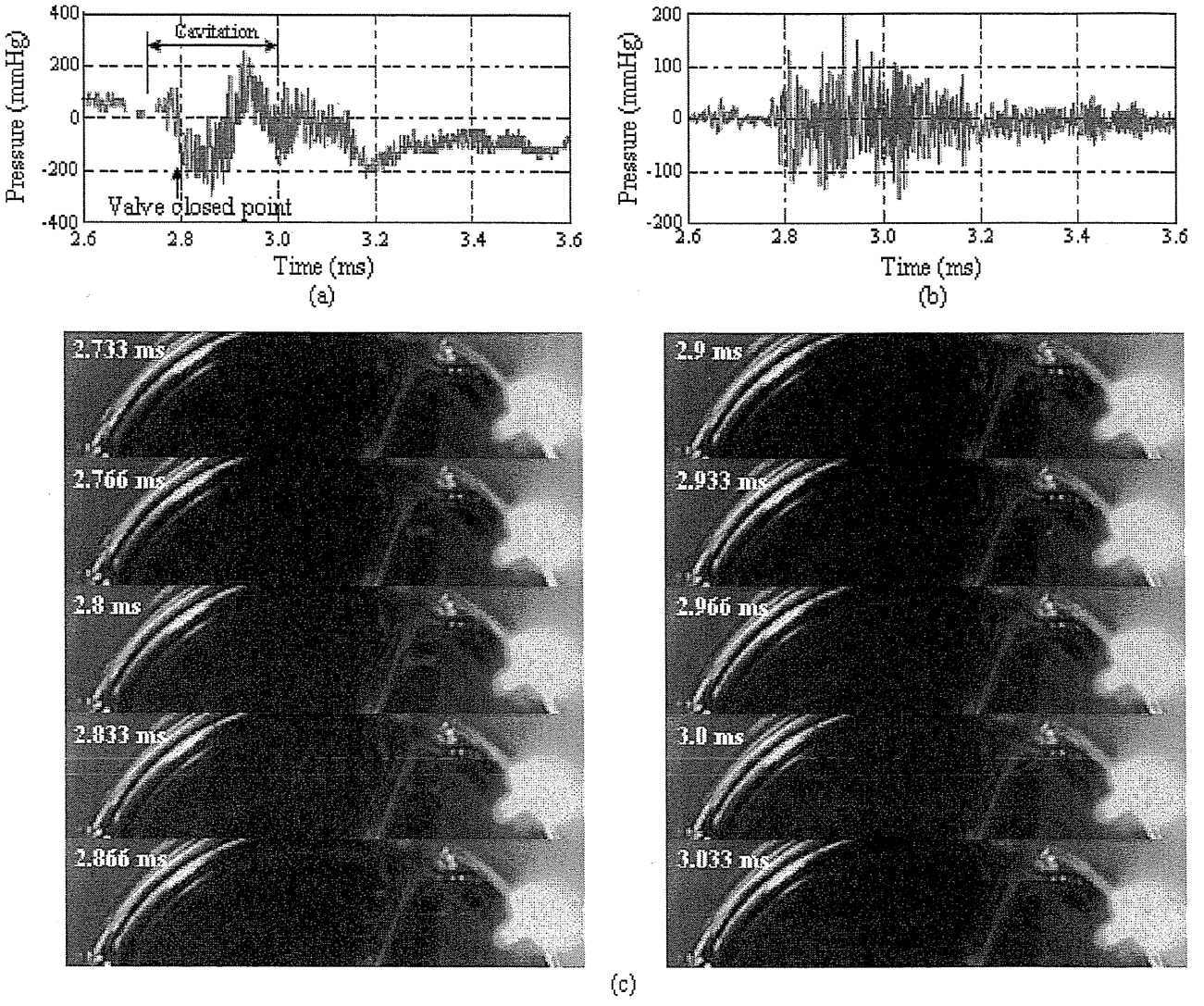

FIG. 7. Cavitation bubbles and pressure signal at a heart rate of 90 bpm. (a) Pressure signal; (b) Band-pass filtered signal; (c) Images of cavitation bubbles.

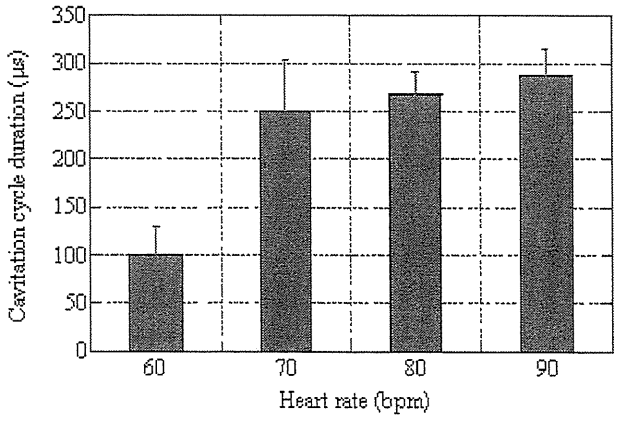

FIG. 8. Cavitation cycle duration. This is equal to the number of frames during which cavitation bubbles were visible multiplied by the interval of the frames.

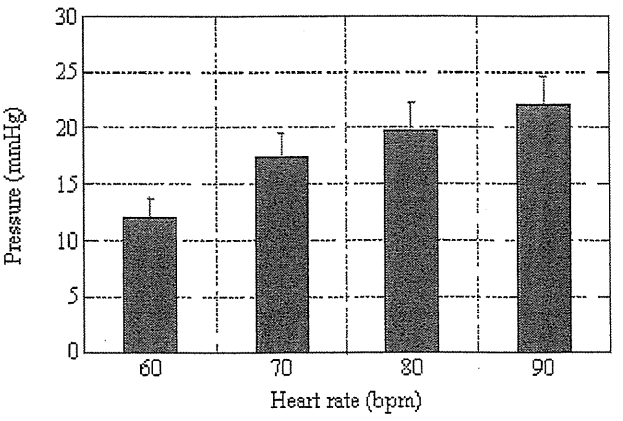

FIG. 9. RMS pressure. This is band-pass filtered between 35 and 200 kHz using a digital filter.